

# Multiperiodicity, modulations and flip-flops in variable star light curves<sup>\*</sup>

## III. Carrier fit analysis of LQ Hya photometry for 1982-2014

N. Olsper<sup>1</sup>, M. J. Käpylä<sup>1</sup>, J. Pelt<sup>2</sup>, E. M. Cole<sup>3</sup>, T. Hackman<sup>3,4</sup>, J. Lehtinen<sup>3</sup>, and G. W. Henry<sup>5</sup>

<sup>1</sup> ReSoLVE Centre of Excellence, Aalto University, Department of Information and Computer Science, PO Box 15400, FI-00076 Aalto, Finland

<sup>2</sup> Tartu Observatory, 61602 Tõravere, Estonia

<sup>3</sup> Department of Physics, PO Box 64, FI-00014 University of Helsinki, Finland

<sup>4</sup> Finnish Centre for Astronomy with ESO (FINCA), University of Turku, Väisäläntie 20, FI-21500 Piikkiö, Finland

<sup>5</sup> Center of Excellence in Information Systems, Tennessee State University, 3500 John A. Merritt Blvd., Box 9501, Nashville, TN 37209, USA

Received / Accepted

### ABSTRACT

**Aims.** We study LQ Hya photometry for 1982-2014 with the carrier fit (hereafter CF) -method and compare our results to earlier photometric analysis and recent Doppler imaging maps.

**Methods.** As the rotation period of the object is not known a priori, we first utilize different types of statistical methods (least-squares fit of harmonics, phase dispersion statistic) to estimate various candidates for the carrier period for the CF method. Secondly, a global fit to the whole data set and local fits to shorter segments are computed with the period that is found to be the optimal one.

**Results.** The harmonic least-squares analysis of all the available data reveals a short period close to 1.6 days as a limiting value for a set of significant frequencies. We interpret this as the rotation period of the spots near the equatorial region. In addition, the distribution of the significant periods is found to be bimodal, hinting of a longer-term modulating period, which we set out to study with a two-harmonic CF model. Weak modulation signal is, indeed retrieved, with a period of roughly 6.9 years. The phase dispersion analysis gives a clear symmetric minimum for coherence times lower than and around 100 days. We interpret this as the mean rotation pattern of the spots. Of these periods, statistically the most significant and physically most plausible is the mean spot rotation period  $1^d60514$ , which is chosen to be used as the carrier period for the CF analysis. With the CF method we seek for any systematic trends in the spot distribution in the global time frame, and locally look for abrupt phase changes earlier reported in rapidly rotating objects. During 2005–2008 the global CF reveals a coherent structure rotating with a period of  $1^d6037$ , while during most other times the spot distribution appears rather random in phase.

**Conclusions.** The evolution of the spot distribution of the object is found to be very chaotic, with no clear signs of an azimuthal dynamo wave that would persist over longer time scales, although the short-lived coherent structures observed occasionally do not rotate with the same speed as the mean spot distribution. The most likely explanation of the bimodal period distribution is attributed to the high- and low latitude spot formation regions confirmed from DI and ZDI.

**Key words.** stars: activity, photometry, starspots, LQ Hya (with HD identifier)

## 1. Introduction

LQ Hya (HD 82558, GL355) is a chromospherically active BY Draconis -type star of the spectral type K2V (Cutispoto 1991; Covino et al. 2001). It also shows a high level of Ca H&K emission ( $\log R'_{\text{HK}} = -4.06$ , White et al. 2007), manifesting very high level of magnetic activity. With an estimated mass of  $0.8 \pm 0.1 M_{\odot}$  and age  $51.0 \pm 17.5$  Myrs (Tetzlaff et al. 2011), the star is considered a young

solar analogue. The star spins very fast, with the estimated rotation period being around 1.6 days (e.g. Jetsu 1993; Berdyugina et al. 2002; Kovári et al. 2004; Lehtinen et al. 2012).

In addition to exhibiting strong magnetic activity indicators, the star shows modulation in its light curve, as first proposed by Eggen (1984) and confirmed by Fekel et al. (1986). Such behavior is interpreted as cool spots rotating with the stellar surface. For this reason photometric light curves have been used to determine the rotation period of the star. If the star exhibits latitudinal and/or radial surface differential rotation analogous to the Sun, or latitudinal dynamo waves (which is the solar case, as the sunspots form the well-known butterfly diagram with cyclic behavior known as Spörer's law) and/or azimuthal dynamo

Send offprint requests to: N. Olsper  
e-mail: nigul.olsper@aalto.fi

\* Based on observations made with the Nordic Optical Telescope, operated on the island of La Palma jointly by Denmark, Finland, Iceland, Norway, and Sweden, in the Spanish Observatorio del Roque de los Muchachos of the Instituto de Astrofísica de Canarias.

waves (which can occur in the rapid rotation regime, e.g. Lindborg et al. 2011), this simple picture might not be applicable. Indeed, based on previous studies of LQ Hya photometry it has become evident that no single period suitable for describing the physical system throughout the whole observational time span available exists. However, for shorter epochs dominating periods have been found. In Jetsu (1993) a good phase coherence was achieved with a period of  $1^d601136$ , Berdyugina et al. (2002) arrived at a period estimate of  $1^d601052$ , Kovári et al. (2004) report a period of  $1^d60066$ , and the analysis of Lehtinen et al. (2012) gives a period  $1^d6043$ .

The surface differential rotation of the object has been estimated by either using photometric lightcurves (Jetsu 1993; Berdyugina et al. 2002; You 2007; Lehtinen et al. 2012), or spectroscopic observations analyzed with Doppler imaging (hereafter DI) methods (Strassmeier et al. 1993; Saar et al. 1994; Rice & Strassmeier 1998; Kovári et al. 2004) and Zeeman Doppler imaging (hereafter ZDI) methods (Saar et al. 1994; Donati 1999; Donati et al. 2003b; McIvor et al. 2004). It is customary to define the differential rotation parameter as

$$k = \frac{\Omega_{\text{eq}} - \Omega_{\text{pole}}}{\Omega_{\text{eq}}} = 1 - \frac{\Omega_{\text{pole}}}{\Omega_{\text{eq}}}, \quad (1)$$

describing both the magnitude and the type of the latitudinal rotation law. Large values of  $k$  denote strong differential rotation, positive signs corresponding to solar-like profiles with a faster equator and a slower pole, negative to anti-solar profiles with faster poles and a slower equator. From photometry, only the magnitude of  $k$  can be deduced, while using DI one can also determine the sign of it. The values obtained from the fluctuations in the photometric period range from  $k = 0.015$  (Jetsu 1993) to 0.025 by (You 2007).

The DI and ZDI results of Saar et al. (1994) initially estimated an upper limit of differential rotation based on polar ‘smearing’ of  $k \lesssim 0.03$  and further analysis by Kovári et al. (2004); Donati et al. (2003a) indicate even weaker ( $k = 0.002\dots 0.006$ ) solar-like differential rotation. Due to the relatively low  $v \sin(i)$  of the object versus the required value for DI techniques, the results show significant scatter (see e.g. Barnes et al. 2005). Obtaining a reliable value for differential rotation using DI and ZDI requires a longer baseline of observations than used in most studies (Strassmeier et al. 1993; Rice & Strassmeier 1998).

In general, the amount of differential rotation in this object can be concluded to be very small compared to the solar value of  $k \approx 0.2$ . Hydrodynamical mean-field modeling of the rotation law of this object by Kitchatinov & Olemskov (2011) agrees with the observations in the sense that the obtained profiles are solar-like, and the magnitude falls within the observational range ( $k = 0.028$ ).

The DI and ZDI maps (e.g. Strassmeier et al. 1993; Saar et al. 1994; Rice & Strassmeier 1998; Donati 1999; Donati et al. 2003b; Cole et al. 2014a) show both high- and low-latitude spot activity on the object to the extent that Cole et al. (2014a) define the distribution over latitude to be bimodal. The relative strength of the two latitudinal spot regions has been reported to be highly variable over time so that during some epochs the near-equator spots dominate while during others the nearly polar features are the strongest. The spot distribution from DI and ZDI has been postulated to be concentrated onto active longitudes during some epochs, therefore being occasionally highly non-

axisymmetric (e.g. Saar et al. 1994), but during different epochs no clear signs of active longitudes have been found (e.g. Cole et al. 2014a).

Many authors of photometric or DI studies have reported the concentrations of the spot activity on certain longitudes (Jetsu 1993; Berdyugina et al. 2002; Kovári et al. 2004; Lehtinen et al. 2012). The periods producing the largest amount of phase clustering and the phase separation of the ‘active longitudes’ vary significantly depending on the data set span and timing, and also the method used, indicating that these structures are not persistent, but rather may be changing strongly in time. For example, Lehtinen et al. (2012) concluded that during 1988–2012, two different periods describing structures with active longitudes  $P_{\text{al}} = 1^d61208$  and  $P_{\text{al}} = 1^d603693$ , the former one appearing around 1995 and the latter one between the years 2003 and 2009, were needed to describe the phase clustering of the data. In contrast, Berdyugina et al. (2002) used a light curve inversion technique to recover spot phases and postulated the existence of two active longitudes about  $180^\circ$  apart, spanning the entire 20 years of the data set, and calculated a new rotation period for the spot structure from the drift of these active longitudes,  $P_{\text{al}} = 1^d601052 \pm 0^d000014$ .

The mean brightness of the star exhibits obvious signs of cyclic activity. Various determinations from photometry indicate cycles of around 6–7 years (e.g. Jetsu 1993; Strassmeier et al. 1997; Cutispoto 1998; Oláh et al. 2009), while also co-existing shorter (of the order of 3 years, e.g. Messina & Guinan 2003) and longer (of the order of 11 years, e.g. Oláh et al. 2000) cycles have been reported. Berdyugina et al. (2002), who postulated coherent active longitudes during the time span of almost 20 years, found a 7.7-year cycle in the mean brightness, and additionally a 5.2-year cycle related to the regular change of the activity level of the two active longitudes (flip-flop).

From the various earlier studies it is evident that the behavior of the object is extremely complex, and a systematic approach to understand these complexities is yet missing in the literature. This is attempted in the current study using the CF method, the essential properties of which are explained in Sect. 3.1. This method has been previously successfully applied to study spot activity in other types of stars: see Hackman et al. (2013) for the analysis of FK Coma Berenices and Lindborg et al. (2013) for the analysis of II Pegasi. As the rotation period of the star is not known *a priori*, we first search for the optimal carrier frequency using different kinds of statistical methods described in Sect. 4.1–4.3. We then perform a global CF using the optimal carrier frequency (Sect. 5.1), the aim being to search for any persistent trends and/or phase disruptions. Finally, we perform local CF-s to study local segments in an attempt to identify interesting phase behavior. Here we also make a comparison to the Continuous Period Search (hereafter CPS) method results by Lehtinen et al. (2012) and the recent DI results of Cole et al. (2014a). In Sect. 6 and Sect. 7 we discuss and conclude our findings.

## 2. Data

In this paper we use the data consisting of nearly 32 years of photometry from three different sources, namely the photometry collected and published in Berdyugina et al. (2002) from HJD = 2 445 275 (2 November 1982) to HJD =

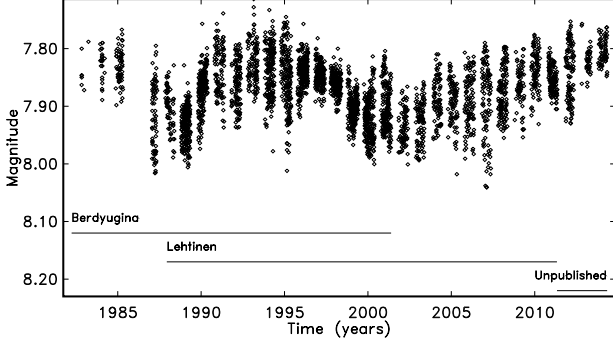


**Fig. 1.** The combined data set from the three different sources. The dataset referred to as D1 consists of all available data, while dataset D2 comprises only T3-APT data (Lehtinen + unpublished).

2 452 053 (23 May 2001), the published photometry of Lehtinen et al. (2012) from HJD = 2 447 141 (11 December 1987) to HJD = 2 455 684 (2 May 2011) obtained with the T3 0.4m APT at the Fairborn Observatory, Arizona and finally unpublished photometry obtained with the same telescope from HJD = 2 455 685 (3 May 2011) to HJD = 2 456 783 (5 May 2014). From these data sources (see Fig. 1) we compiled two input data sets. First we rescaled T3-APT data to fit the data from Berdyugina et al. (2002) and for overlapping observations, computed data points as averages (maximum allowed time difference of 0.1 days was used). As a result of this procedure we got a long data set (hence D1) consisting of 3929 observations covering 11508 days. This data set was used to perform periodicity analysis and optimal carrier period value estimation, the analysis presented in Sect. 4. For the CF analysis presented in Sect. 5, we combined all data from T3-APT telescope, i.e. the data published in Lehtinen et al. (2012) supplemented with the seasons up to May 2014. As a result we got a homogeneous data set (hence D2) which consisted of 2907 observations covering 9642 days. We denote this data set as homogeneous, as it was observed with the same instrument with the same comparison star (HD 82428). We also note that it is of better quality than the D1 data.

### 3. Carrier fit method

#### 3.1. Overview

A detailed description and the discussion of applicability of the CF method can be found in Pelt et al. (2011); here we briefly cover some of the key aspects of it. A CF model can be described as a truncated slowly modulated harmonic decomposition of the signal:

$$f(t) = a_0(t) + \sum_{k=1}^K (a_k(t) \cos(2\pi t k \nu_0) + b_k(t) \sin(2\pi t k \nu_0)), \quad (2)$$

where  $\nu_0$  is the carrier frequency,  $a_0(t)$  is the time-dependent mean level of the signal,  $K$  is the total number of harmonics included in the model, describing the overtones of the basic carrier frequency.  $a_k(t)$  and  $b_k(t)$  are

the low-frequency signal components which can be modeled by either splines or harmonics. Depending on the time series in question, either one of these approaches may be a more suitable choice, e.g. the spline approximation might be more suitable for cases where the signal is known to abruptly change. However, generally the difference between goodness of fits (for definition, see Sect. 3.2) is marginal in case the number of free parameters for both methods are of the same order. In the scope of the current study we limit ourselves to the option of harmonic modulators.

The value for the carrier frequency used in the above model can be, for instance, the rotation period of the object, or any other clocking frequency describing the system. In case of LQ Hya, however, the rotation period is not directly known, as it is a single star. Therefore, we discuss various approaches to carrier frequency (or period) selection below.

Following the notation used in Pelt et al. (2011), the trigonometric approximation of the slow amplitude modulation curves can be written as:

$$a(t) = c_0^a + \sum_{l=1}^L (c_l^a \cos(2\pi t l \nu_D) + s_l^a \sin(2\pi t l \nu_D)), \quad (3)$$

$$b(t) = c_0^b + \sum_{l=1}^L (c_l^b \cos(2\pi t l \nu_D) + s_l^b \sin(2\pi t l \nu_D)), \quad (4)$$

where  $L$  is the total number of harmonics used in the modulator model and  $\nu_D = 1/D = 1/C \cdot (t_{\max} - t_{\min})$ , where  $D$  is data period,  $C$  is the coverage factor and  $[t_{\min}, t_{\max}]$  is the time interval to be fitted with the model. Here we note that the data period  $D$  must be significantly longer than the carrier period  $P_0 = 1/\nu_0$ , and preferably also be a little longer than the actual time span of the data, i.e. the coverage factor should be  $C \gtrsim 1$ .

#### 3.2. Selection of free parameters

One of the crucial things to consider when applying the CF method to real data is the suitable values of the free parameters ( $\nu_0$ ,  $K$ ,  $L$  and  $C$ ). As the selection of the carrier frequency  $\nu_0$  is particularly important we dedicate the whole of the Sect. 4 to it. The methods used for determining the values for other parameters will be discussed here. In general we need to run the computations with all possible combinations of parameter values drawn from some meaningful ranges and then estimate the goodness of fit for every run using

$$R^2 = 1 - \frac{\sum_{i=1}^n (y_i - f_i)^2}{\sum_{i=1}^n (y_i - \bar{y})^2}, \quad (5)$$

where  $n$  is the number of data points,  $y_i$  is the value of the  $i$ -th data point,  $f_i$  is the value of the fit corresponding to the time moment of  $i$ -th data point and  $\bar{y}$  is the mean of the values of all data points. Qualitatively speaking the goodness of fit compares the variance of data points around the model to that one of the data itself. In the current study we use two approaches: we start by analyzing the full set of data as a whole (global fit) followed by the analysis of seasonal data segments (local fit). In both cases we aim at

as high  $R^2$  values as possible while avoiding the possibility of either overfitting the data or fitting into the gaps.

Before continuing with the methods of parameter selection we note that the suitable value for  $L$  is first of all dependent on the value of the coverage factor  $C$ , which defines the period of the slowest modulator in the model. It is reasonable to adopt a value of the same order or little longer than the length of the whole data set. This way we guarantee that the slowest detectable changes in the data are taken into account by the model. In the current study we have fixed  $C = 1.2$ .

The difficulty introduced by the gaps in the data constitutes the so called cycle count problem. The low frequency modulators  $L$  introduce variance around the carrier frequency. Here, we need to keep in mind that the difference in cycle counts for these maximum and minimum frequencies during the longest gap in the data should be less than one to avoid phase match indeterminacy. This can be concisely expressed by the following criterion:  $(\nu_0 + \nu_D)\Delta_{\text{gap}} - (\nu_0 - \nu_D)\Delta_{\text{gap}} < 1$ , where  $\nu_0$  is a high frequency carrier,  $\nu_D$  is a low frequency modulator and  $\Delta_{\text{gap}}$  is the length of the longest gap in the given data set. After making replacement  $\nu_D = L/D = L/C \cdot (t_{\text{max}} - t_{\text{min}})$  and simplifications we obtain an estimate for the upper limit of  $L$ :

$$\frac{2L \cdot \Delta_{\text{gap}}}{C \cdot (t_{\text{max}} - t_{\text{min}})} < 1 \Rightarrow L < \frac{C \cdot (t_{\text{max}} - t_{\text{min}})}{2 \cdot \Delta_{\text{gap}}}. \quad (6)$$

Using this formula we can estimate the maximum valid  $L$  for the data set with the given time span and the longest gap.

In case of local fits, due to the low number of data points the possibility of an overfit appears. We use Bayesian information criterion (hereafter BIC) to determine the optimal values for  $K$  and  $L$  in a similar way it was done in Lehtinen et al. (2011), the differences being that we have 2 parameters in the model and we omit the weights of the data points. More precisely, we search for the minimum of the following criterion:

$$R_{\text{BIC}} = n \ln(\sigma^2) + ((2 + 4L)K + 2L + 1) \ln n, \quad (7)$$

where  $\sigma^2 = \frac{1}{n-1} \sum_{i=1}^n (y_i - f_i)^2$  and we have used the same notation as in Eq. (5). The first term of this equation describes the quality of the fit and the second one adds a penalty proportional to the total number of parameters in the model. Now, as we need the information for possible primary and secondary minima to be able to detect flip-flop type events, we omit  $K = 1$  from the set of trial values. For  $L$  we don't impose a lower limit, but we will calculate the upper limit using Eq. (6) to check if the value obtained from BIC is valid. If it exceeds the upper limit, we will use the latter one as the optimal value. The practical application of this procedure is detailed in Sect. 5.2.

In case of the global fit the possibility of overfitting is quite low as the presence of long seasonal gaps in the data significantly lowers the maximum possible values for  $K$  and  $L$ . It is quite probable that when increasing the number of parameters, the model starts showing big distortions in the regions where data is missing, considerably earlier than high value of  $R^2$  (e.g. 90 %) is achieved.

Before starting to measure the effect of the gaps on the model, we first need to specify how long a region without

data qualifies as a gap. In our case the data is divided into observational seasons where relatively densely spaced data is alternating with a bit shorter ranges with no data at all. Based on a closer look at the actual spacing of the data we define the gap as any region without data that is longer than 130 days. This definition leads to 27 segments with data and 26 gaps between them (minimum being 139 and maximum 302 days). The length of the homogeneous data set is 9642 days, thus using Eq. (6) with the maximal gap size of 302 days we obtain a maximum value for  $L$  to be 19. As explained in Sect. 4.1 this is too low value to cover the full spectrum of the data. Here we stand in front of the question either to leave out the data points preceding the longest gap or lose the reliability of the model during this single gap while still obtaining better overall results. In the current study we decided to choose the latter option. The second longest gap in the data is 192 days long, increasing the suitable value for  $L$  to 30. This number is already in the same order as the number of observing seasons, so that we could expect good approximation of the seasonal variation by the term  $a_0(t)$  in Eq. (2).

In choosing the suitable values of high frequency components  $K$ , there is not much room for us: on one hand  $K = 2$  is the lowest value meaningful in our analysis due to the same considerations as pointed out in case of the local fits. On the other hand tests with  $K = 3$  showed only a small positive effect in the achieved  $R^2$  value while significantly increasing the freedom of the model (distortions) in the region of gaps. Based on these arguments we decided to fix  $K = 2$ . Total number of parameters in our model is therefore 305, which means approximately 10 data points per parameter.

After the optimal parameter values for the model have been fixed the goodness of fit can be further increased by removing the  $3\sigma$  outliers to the initial fit from the data and then refitting again. The outliers can be either observationally unreliable points or possible flares such as that one around April 2000 or HJD 2451650. In our case total of 22 outliers were detected. Removal of these leads to approximately 3% increase in  $R^2$  for global fit. Therefore in all subsequent CF analysis (for global as well as for local) we have used the data set with outliers eliminated.

### 3.3. Visualization

For visualizing the CF model we use the same technique as introduced in Pelt et al. (2011, p. 4, sect 2.6). Firstly, we divide the whole time span into number of bins with the length of the chosen carrier period. Secondly, for each bin we normalize the signal amplitude into range  $[-1, 1]$  and then plot it with the corresponding time moment of the bin and the phase relative to the carrier period. This normalization step is useful for making the phase behavior of the signal comparable over the whole time span. Without normalization the features during high amplitudes will dominate the picture. Here we use both approaches for the purpose of obtaining more information about the processes governing the star. At the bottom of the plot we include a so-called 'bar-code' to give information of the density of the data points around the given time moments. Black indicates densely spaced data, while yellow indicates sparsely spaced or no data at all. Some previous examples using the given technique can be found in (Hackman et al. 2013; Lindborg et al. 2013).

### 3.4. Minima detection, error and significance estimation

Besides using CF method for visualizing the results, we determine primary and secondary minima from the model of global fit and compare them to results obtained from DI analysis and the earlier analysis of a shorter segment of the same data used here with a different method (CPS; (Lehtinen et al. 2012)). Error estimates for the minima are calculated by generating 1000 bootstrap samples from the original data (by reshuffling the residuals of the data points to the initial CF model allowing recurrences), repeating the CF analysis for each new data set, and finally, obtaining the distributions for the minima. We mark a minimum as being reliable if and only if the following two conditions are satisfied for distributions both in time and magnitude: the Kolmogorov-Smirnov test with preassigned significance level 0.01 against a normal distribution must pass and the bias of the mean of the distribution from the original estimate should be less than the standard deviation of the distribution. The error and significance estimates for each minimum are given in the electronic material containing the full global fit.

## 4. Methods and results for searching the optimal carrier frequency

The selection of the optimal carrier frequency to analyze LQ Hya light curves is far from a trivial task. There is a wide range of different periods obtained from different data sets and by using different methods. This is why we need a thorough analysis of the periods to proceed with the CF method.

Taking off from the solar analogy, one might hypothesize that there are at least four types of periodicities that one needs to deal with:

1. Behind all the observable activity is the stellar surface rotation and its non-uniformities. In the solar case, the sunspots rather closely follow the motion of the solar surface seen from Dopplerograms; the only exception are the longitudinal activity nests that have been reported to show motions that differ from the general pattern. In the absence of asteroseismic data, it is impossible to distinguish between the motion of the plasma and the spots themselves, and the determination of the rotation period is out of the scope of this study.
2. Through photometry, one can hope at least to be able to determine the mean rotation period of the spots on the stellar surface, analogous to the Carrington rotation period of the Sun.
3. Using the DI and ZDI results of significant spot activity in the low-latitude regions and solar-like rotation law of LQ Hya as valid assumptions one may also be able to determine the spot rotation period near the equatorial region, as this should arguably be the shortest period of rotational origin seen in the periodograms.
4. Analogously to the periods derived for the longitudinal activity nest on the solar surface for the azimuthal dynamo waves on some more evolved rapid rotators, photometric studies can be used to determine whether any longitudinal clustering occurs and does the period of the active longitudes differ from the mean rotation period of the spot distribution.

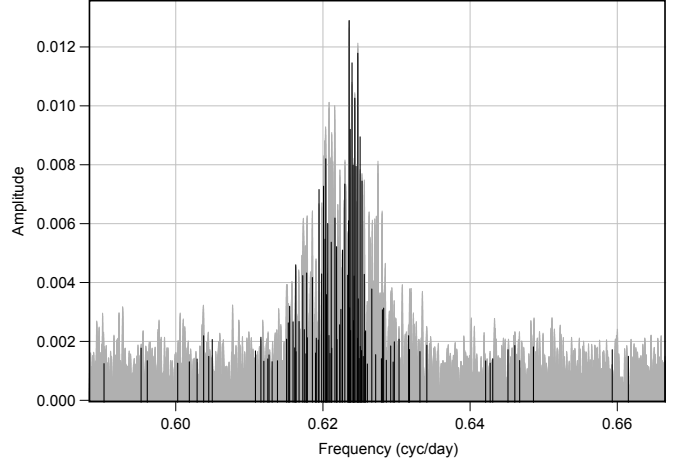


**Fig. 2.** Amplitude spectrum for the important period range 1.5-1.7 days (gray) and first 100 frequencies obtained by sequential prewhitening procedure (black).

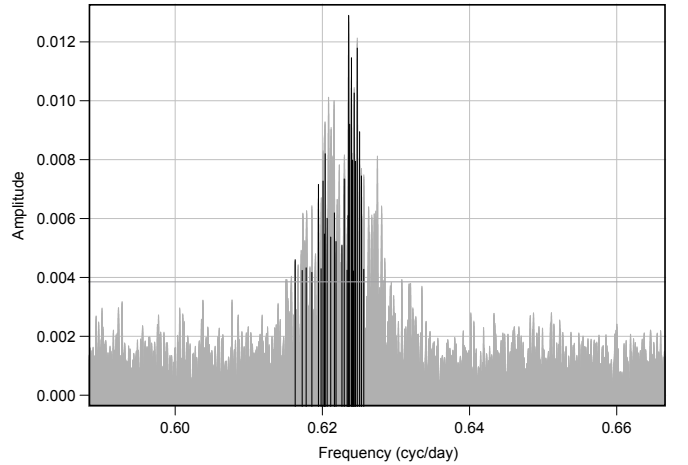


**Fig. 3.** The set of 28 strongest amplitudes (black) and original amplitude spectrum (gray). The horizontal line marks the cut-off level obtained from 100 randomized samples.

### 4.1. Least-squares fitting

For irregularly spaced data sets the most common procedure of frequency analysis is a simple least-squares fit of a harmonic waveform into the data with the range of some trial periods. The particular computational schemes and descriptive statistics vary (see e.g. Barning 1963; Lomb 1976; Scargle 1982). In our analysis we chose the simplest statistic which measures the relevance of the harmonic under discussion, namely its amplitude.

Before computing the amplitude spectrum, we removed the seasonal means (de-trending) of the full LQ Hya V-band photometry data. The complexity of the spectrum, depicted in Fig. 2 with gray color, is obvious and it is very hard to single out any prominent peak from the forest of peaks in it. The analysis can and must be improved by removing the spurious periods rising from the gapped nature of the data. For this, we used the so called pre-whitening

Period	Previous estimates	Source
1.601279	1.601136	(Jetsu 1993)
	1.601052	(Berdyugina et al. 2002)
1.600662	1.600881	(Strassmeier et al. 1997)
	1.600834	(Berdyugina et al. 2002)
	1.60066	(Kovári et al. 2004)
1.603893	1.6042	(Messina & Guinan 2003)
	1.60369	(Lehtinen et al. 2012)

**Table 1.** Periods with strongest peaks in the spectrum compared to previous estimates

method (for a recent application of the method, see e.g. Reinhold & Reiners 2013). We iteratively removed most significant harmonics with estimated amplitudes, and proceeded in the next step with the least squares fit residuals. In this way we computed a set of 100 strongest amplitudes which are depicted in Fig. 2 with black color. These are not, with high probability, aliases due to the most prominent yearly gap structure with frequency offsets of  $\Delta\nu \approx 1/365$ . Even after this cleaning procedure, we still have a very complex set of different frequencies.

A large part of the estimated frequencies with corresponding amplitudes are well below the noise level and we can disregard them. To estimate a suitable cut off level, below which the peaks are considered insignificant, we proceeded in the following way. We built artificial data sets from the original by reshuffling them in time. For every new data set we found its strongest peak. The amplitude cut off level was then chosen as a value of maximum amplitude in 100 different such random runs. This criterion is rather conservative and we can be quite confident that the 28 periods, shown with black lines in Fig. 3, whose amplitudes occurred to be higher than the cut off level (0.00385; indicated with a horizontal line in Fig. 3) are not the results of random fluctuations. As seen from the plot, the set of the selected peaks is now much more localized. Among the peaks are practically all the periods which have been proposed so far by different authors for different data sets, see Table 1.

The selected set of periods lay in the interval 1.598406...1.622572 days (or in frequency terms 0.6163053...0.6256234 cycles per day). The center of the full range interval is at  $\nu_0^{\text{LS}} = 0.6209644$  ( $P_0^{\text{LS}} = 1^{\text{d}}6103984$ ) and this is the first logical candidate for the carrier frequency. The logic behind this choice would be obvious - the full frequency range will be covered on equal grounds.

Several authors have already reported on the period variability of LQ Hya. By using local fits, e.g. Messina & Guinan (2003) give period in the range  $1^{\text{d}}5938 - 1^{\text{d}}6154$  and You (2007) report  $1^{\text{d}}60094 - 1^{\text{d}}60918$  range from their analysis. The obtained range of periods is also in good agreement with a set of rotation periods obtained from a simple spot modeling procedure by Alekseev (2005). The time span for our main homogeneous data set (D2) is around 9642 days. Correspondingly the range of rotation counts for the significant periods is 5942...6032 with a difference of 90 rotations. For the carrier frequency around the center of the estimated range this allows up to 45 full phase cycle runs in both directions. In Sect. 3.2, however, we concluded that the optimal harmonic count for low frequency modulation curve is around 30 cycles. From this follows that in principle the very sharp (momentous) fre-

quency jumps from one side of the range to the other can become smoothed out to some extent.

On the other hand, the second longest seasonal gaps in the data is around 192 days and corresponding cycle counts are 199...120 Obviously, for the carrier periods in the middle of the full range the phase migration during the gaps is certainly less than a full turn, cf. Eq. (6). For the longest gap in the data (around 300 days), however, we can theoretically have a cycle count error and consequently the approximated solution in this region can not be regarded reliable.

Finally, one interesting observation that can be seen in Fig. 3 is that the distribution of the significant frequencies is bimodal, i.e. there are two bunches of them. Interestingly enough, as seen from Table 1 typical solutions are concentrated in the rightmost bunch of periods, the cut-off being very sharp on the higher frequency (shorter period) side.

The bimodal structure of the period distribution leads us to another trial hypothesis - that we have here a case when a certain frequency in between the two bunches is more or less periodically modulated (with period around 2000-3000 days). This hypothesis was already set up in an earlier paper (see Berdyugina et al. 2002). To check it once again we carried out the corresponding analysis for our significantly longer data set D2.

#### 4.2. Carrier from a multiperiodic model

The simplest conceivable model for the slowly modulated signal is a time series which depends on the carrier period  $P_0^{\text{MP}} = 1/\nu_0^{\text{MP}}$  and modulating period  $P_{\text{mod}} = 1/\nu_{\text{mod}}$  in a coupled way. That means that all positive combination frequencies

$$\nu_{i,j} = i \times \nu_0^{\text{MP}} + j \times \nu_{\text{mod}}, i, j = -N, \dots, N, \quad (8)$$

can take part in waveforming. In the simplest case of  $N = 2$  there will essentially be 25 different trigonometric terms (constant included) which must be fitted into the observed data using the least squares method (see Berdyugina et al. 2002). The periods producing the best fit will then used to build final model.

We performed this kind of analysis for the data set D2. The resulting pair of periods occurred to be  $P_0^{\text{MP}} = 1^{\text{d}}602680 \pm 0^{\text{d}}0000027$  and  $P_{\text{mod}} = 2534^{\text{d}}6 \pm 6^{\text{d}}6$  (roughly 6.94 years). The resulting fit can be visualized by the same devices as the carrier fit. We divide the solution into period length fragments and stack them properly. In Fig. 4 our solution is depicted. The  $R^2$  value for the least squares fit for these two periods is quite low (23.6%). However, it is remarkable that the modulation period is very similar to values often quoted as the long cycle length of LQ Hya (e.g. Jetsu 1993; Oláh et al. 2000; Berdyugina et al. 2002; Alekseev 2005).

If we now base our consideration on the idea that the possible doubly periodic component is a relevant aspect of the overall variability then we can use the computed carrier value as a model based carrier  $P_0^{\text{MP}}$  for the CF procedure. The result of this analysis is shown in Fig. 5. Unfortunately, the regular structure of the simple model is largely lost and a number of other variability elements dominate the picture.



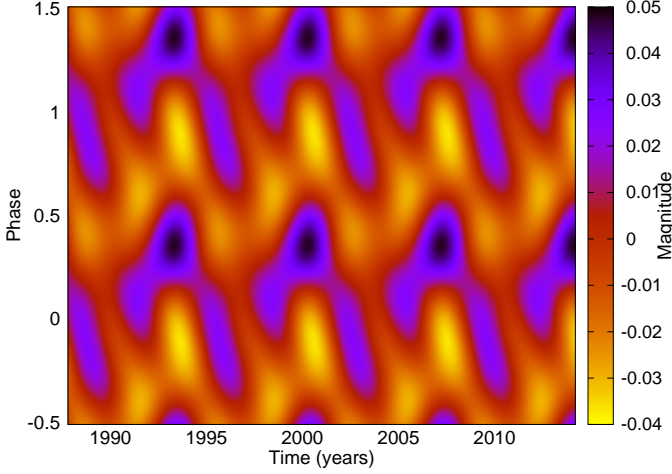


**Fig. 4.** Folded and stacked light curve model with periods  $P_0^{\text{MP}} = 1^{\text{d}}602680$  and  $P_m = 2534^{\text{d}}6$ . This regular structure helps to describe only  $R^2 = 23.542\%$  of overall variability.

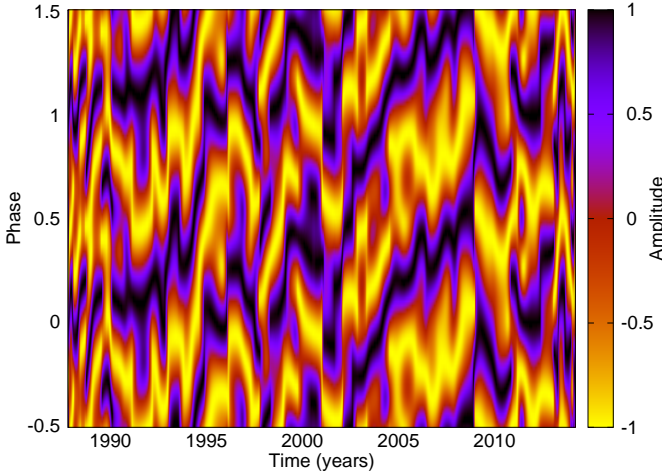


**Fig. 5.** Carrier fit obtained with the carrier  $P_0^{\text{MP}} = 1^{\text{d}}60268$  obtained from the two-periodic model of Sect. 4.2

### 4.3. Carrier from the phase dispersion analysis

From Fig. 3 we can well see that the period computed as a mean from the formal range of significant periods is not very representative due to the bimodal nature of the distribution. This is also true if the peak with maximum amplitude was selected as a carrier. Slightly better method would be the one used in Lehtinen et al. (2012) where the best period was selected using phase distributions of the light curve extrema. However in this case the interplay between different frequencies can shift minima or maxima and obscure the general picture.

To our understanding, the best method for computing the mean period of spots comes from phase dispersion anal-

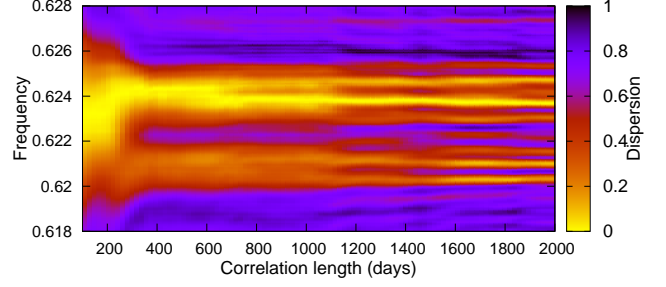


**Fig. 6.** Phase dispersion statistic  $D^2(P)$  for a range of correlation lengths. The dispersion spectrum becomes strongly asymmetric around 230 days and then splits into set of peaks.

ysis (Pelt 1983; Lindborg et al. 2013). It is based on the following simple statistic:

$$D^2(P) = \frac{1}{2\sigma^2} \frac{\sum_{i=1}^{N-1} \sum_{j=i+1}^N g(t_i, t_j, P, \Delta t) [f(t_i) - f(t_j)]^2}{\sum_{i=1}^{N-1} \sum_{j=i+1}^N g(t_i, t_j, P, \Delta t)}, \quad (9)$$

where  $f(t_i), i = 1, \dots, N$  is the input time series,  $\sigma^2$  is its variance,  $g(t_i, t_j, P, \Delta t)$  is the selection function which is significantly greater than zero only when

$$t_j - t_i \approx kP, k = \pm 1, \pm 2, \dots \quad \text{and} \quad (10)$$

$$|t_j - t_i| \leq \Delta t. \quad (11)$$

In the latter condition  $\Delta t$  is so called *correlation length*. For the particular case when  $\Delta t$  is longer than the full data span the  $D^2(P)$  statistic is essentially a slight reformulation of the well known Stellingwerf statistic (Stellingwerf 1978). As the correlation length is made shorter, we match nearby cycles in a progressively narrower region, and consequently estimate a certain mean period, which needs not to be coherent for the full time span. This is well illustrated in Fig. 6, where we show the  $D^2(P)$  statistic for the range of trial frequencies as function of the correlation length,  $\Delta t$ , using color contours. We see that for a small enough correlation length the  $D^2(P)$  statistic yields a rather symmetric single minimum. Above that limit the frequency spectrum starts to distort and eventually splits into separate branches. Finally at large correlation lengths we obtain a forest of minima similar to the results presented in Sect. 4.1. We interpret this behavior in the following way: for short coherence times, the periodogram is dominated by the mean pattern of spot motions, while at longer coherence times the signatures of more persistent spot structures, the rotation of which differs from the mean spot flow, take over and give the strongest signal.

Our aim is to determine the limiting correlation length at which a single minimum is still obtained and use the corresponding period of the phase dispersion minimum as a plausible carrier period. Here we must point out two problems: firstly the minimum of  $D^2(P)$  statistic is usually very wide, and secondly the shape of the peak somewhat deviates from symmetric form (see for details Fig. 7). This prevents us from determining a sufficiently accurate

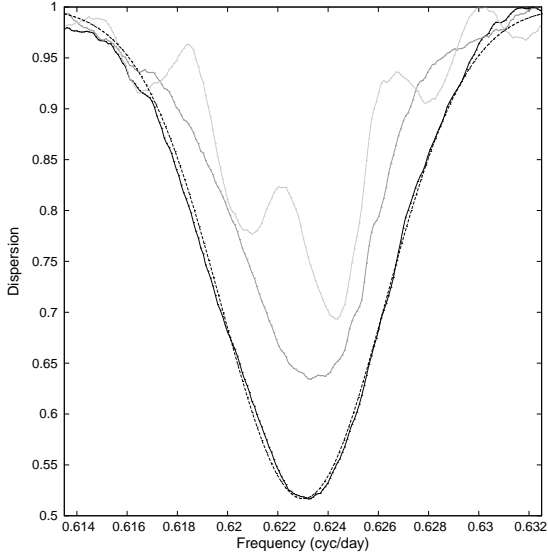


**Fig. 7.** Curves of the phase dispersion statistic  $D^2(P)$  for different correlation lengths in days: 100 (black), 200 (gray) and 300 (light gray). Dashed curve corresponds to the best-fitting Gaussian to the curve with correlation length 100 days.

value of the minimum directly from the curve of the statistic. Instead of that we fit Gaussian profile to the curve of  $D^2(P)$  statistic. Our task is to estimate the free parameters of this gaussian curve (mean  $\mu$  and variance  $\sigma^2$ ) for which the distance to the curve of the  $D^2(P)$  statistic is minimal. The value of the mean obtained this way represents the optimal carrier frequency and the variance represents the scatter of the periods around it. From our analysis it turns out that with the correlation length of 100 days the curve of the  $D^2(P)$  statistic is singular and still symmetric enough, due to which we choose this correlation length as the limiting one, and determine the mean period from this curve. The best-fitting Gaussian has the mean  $\mu = 0.62300$  and standard deviation  $\sigma = 0.00325$  (both in cycles per day). In the time domain the corresponding values are  $P_0^{\text{D}^2} = 1^{\text{d}}60514$  and  $\Delta P_0^{\text{D}^2} \approx 0^{\text{d}}0084$ . For comparison, quite a similar value,  $P_w = 1^{\text{d}}6043$ , was obtained by Lehtinen et al. (2012) by calculating the weighted mean of the periods determined for independent subsets of the whole data.

In the current study we estimated the significance of the mean cycle length  $P_0^{\text{D}^2}$  by testing the null hypothesis that the peak of the minimum is drawn from the distribution of random fluctuations. For that purpose we generated 1000 samples from the original data set via reshuffling the measured magnitudes and then calculated the value of the  $D^2(P)$  statistic for each new data set using correlation length of 100 days. In such a way we obtained a distribution for the minimum of the  $D^2(P)$  statistic caused by random fluctuations. The results showed that in our case the null hypothesis can be rejected with preassigned significance level of 0.05 as the minimum of the  $D^2(P)$  for the original data remains well below the 995th value from the sample distribution which was located around 0.97.

We believe that the carrier value obtained by using the  $D^2(P)$  statistic, which is computed for short correlation

lengths, is well grounded. The other values (the strongest peak in the spectrum, central value of the range, mean value of the set of periods, periods based on extrema) tend to bring in an amount of contingency, as using any of them would in practice mean choosing a certain locally active period for the CF analysis of a global nature.

## 5. CF results

In the following we will use the obtained mean cycle length period of the spots  $P_0^{\text{D}^2}$  as the carrier period, and compute a global as well as local fits based on it.

### 5.1. Global fit

We perform a global CF analysis with the selected parameters  $P_0^{\text{D}^2}$ ,  $K = 2$ ,  $L = 30$ , and  $C = 1.2$ , which gives a model with  $R^2 = 91.7\%$ . Consequently, the carrier fit model describes a rather large part of the overall input data variability. The resulting phase diagram is displayed in Fig. 8, wherefrom it is evident that the phase behavior is characterized by up- and downward trends, while epochs during which the minima would occur at constant phases are almost totally absent. On one hand the slopes of the trends correspond to the different periods, on the other hand the lengths and the locations of the trends give hints of the "duty times" of these cycles (in other words when and for how long these periods dominate). The most noticeable features are two downward trends during the years 2005 – 2008 and 1991 – 1993. These correspond to the periods  $1^{\text{d}}6037$  and  $1^{\text{d}}6026$  days accordingly, which belong to the strongest peaks found previously by frequency analysis. During other epochs the phase behavior is changing more rapidly in time while the abrupt phase shifts seem to appear over the whole time span, even during the strongest trends.

### 5.2. Local fits

In the current study local analysis of the data is carried out mainly for the purpose of visualizing the phase behavior of the signal in more detail than it is possible with the global analysis. Due to insufficient number of modulators in the global fit, the whole spectrum of the data is not covered. This leads to the smoothing of the real signal on small time scales. To get better results we perform a local CF analysis similarly as it was done in Hackman et al. (2013) and Lindborg et al. (2013). Segments contain relatively low number of data points and in some cases considerable gaps are present, thus the maximum allowed number of modulators is significantly smaller than that one for the global fit. Therefore one could assume that no higher precision in the results is achievable. However, the reality is exactly the opposite, we obtain better coverage of the spectrum due to 2 reasons: firstly the spectrum of each segment separately is narrower than that one of the whole data set and secondly the frequencies of the modulators in the model are much higher than the ones used in case of the global fit.

Splitting the data into segments suitable for the local analysis is done using the following rules: we start with the earliest data point and calculate the difference in time between pairs of data points next to each other  $d_i = t_i - t_{i-1}$ . If  $d_i < 100d$  the data point at  $t_i$  is added to the segment, otherwise a new segment is started and the process



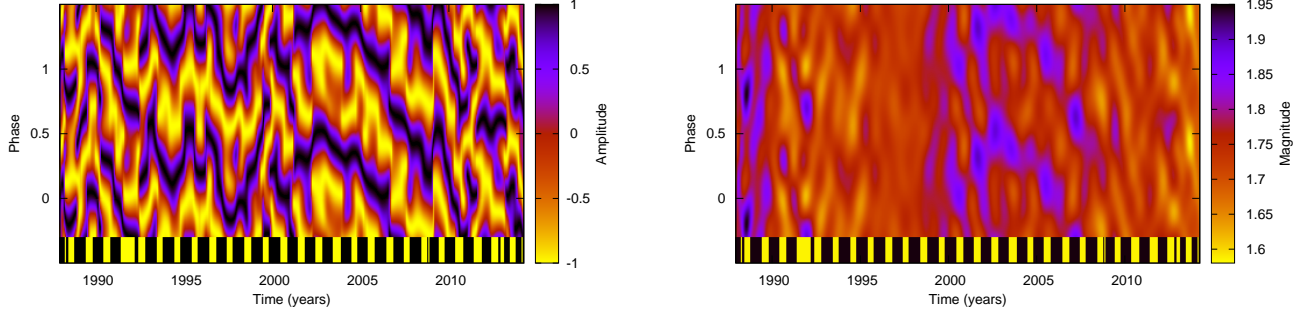


**Fig. 8.** Phase diagram for global fit with carrier period  $P_0^{D2} = 1^d60514$ ,  $K=2$  and  $L=30$ . On left with normalized amplitudes, on right with actual magnitudes

is repeated. Using the above algorithm we obtained 27 segments, the details of which are given in Table 2. CF-s for each segment were applied with the period of the mean cycle length  $P_0^{D2} = 1^d60514$ . The number of harmonics  $K$  and modulators  $L$  optimal for each segment were determined by finding the minimum for the BIC. For all segments  $K = 2$  turned out to be suitable except for the segment 5, which had only 27 points so that realistic modeling was impossible. Due to the cycle count problem  $L$  was further decreased for the segments 1 and 26. Exact number of parameters  $L$  used in the model and the  $R^2$  value achieved for each segment are summarized in Table 2. We can see that for most of the segments the goodness of fit is even higher than 90%, but for segments 3, 10, 11 and 26 it is quite low. In case of the segment 26 this can be explained by a big gap in the data and the low number of points. The other above mentioned three segments are, however, quite densely populated. This might be an indication that the signal is more complex in these segments than what is possible to model with given number of data points. The resulting phase diagrams for all 27 segments are shown in Fig. 9, where the primary minima can be found by following black or dark blue features, while secondary minima appear either as red features between yellow features, or violet features between red features.

In Table 2 occurrences of flip-flops are marked with the '+' symbol, totaling to 4 events in segments 2, 11, 13 and 24. Other type of disrupted phase behavior events are marked with '?', constituting the segments 1, 6, 8, 9, 12, 15, 22, 24 and 27. These are either single phase jumps of primary minima or swaps between primary and secondary minima less than 0.5 in phase. Clear upward trends can be seen in segments 6, 12, 14, 15, 22 and a relatively gentle downward trend in segment 16. These are marked with the symbol '/' in the same table.

A similar analysis was carried out by Lehtinen et al. (2012) using the CPS method for the same data set, except for the last three seasons. The results of this study are in agreement with ours – most of the interesting features can be seen on the phase plots from both studies. Some differences occur for the segments 3 and 6 where some of the minima detected by CF are absent in the case of CPS. For segment 19 there is no secondary minima from CPS, but it can be seen during the first 20 days in case of CF.

No comparison between the results is available for segments 4 and 5 due to low number of data points.

We have calculated epochs of possible flip-flop events also from the global fit using the definition from Hackman et al. (2013):

- the region of main activity shifts about 180 degrees from the old active longitude and then stays on the new active longitude or
- the primary and secondary minima are first separated by about 180 degrees, after which the secondary minimum evolves into a long-lived primary minimum, and vice versa.

Two additional restrictions were added to the above scheme: firstly, we counted only those events for which the phase shift lies between 0.45 and 0.5; secondly, the primary and secondary minima at the moment of flip-flop must be reliable according to the error estimates from bootstrap runs. The results show that four of the total six flip-flop events detected from global CF reside within the data, while two occur in gaps. Moreover, three of these are located in the segments 2, 13 and 24 for which we have detected flip-flops also from local fits. One of the flip-flops, namely within segment 11, was detectable only from the local fit. The epochs of all 7 detected events are depicted in Fig. 10 with thick green vertical lines. Example of the global CF model around the flip-flop event in segment 2 can be seen in Fig. 11. Following the light curve from left to right we notice that the magnitude of the primary minima decreases while that one of the secondary minima increases. After around HJD 2447490 both minima "swap" their magnitudes, the change in phase corresponding to 0.5.

In Berdyugina et al. (2002) a 5.2 year flip-flop cycle was reported. In the light of our current study this periodicity cannot be confirmed: on one hand this is due to the small number of events detected and on the other hand some of the detected events are separated only by 2 or 3 years.

### 5.3. Comparison with Doppler Imaging

Using our CF model for a global fit with the period of mean cycle length of  $1^d60514$  we determined the epochs of primary and secondary minima. In Fig. 10 these epochs are plotted against the phase of the same period. Larger red

Segment	HJD - 2400000 (Date)	$\Delta T_{seg}$	$\Delta T_{gap}$	$N$	$L$	$R^2$	Events
1	47141 (1987-12-11) - 47304 (1988-05-22)	164	47	42	2	96%	?
2	47460 (1988-10-25) - 47660 (1989-05-13)	201	8	215	1	80%	+
3	47832 (1989-11-01) - 48027 (1990-05-15)	196	13	166	1	65%	-
4	48189 (1990-10-24) - 48394 (1991-05-17)	206	39	46	1	93%	-
5	48696 (1992-03-14) - 48759 (1992-05-16)	64	14	27	NA	NA	NA
6	48911 (1992-10-15) - 49132 (1993-05-24)	222	19	88	2	89%	?, /
7	49277 (1993-10-16) - 49499 (1994-05-26)	223	8	137	2	96%	-
8	49645 (1994-10-19) - 49866 (1995-05-28)	222	14	129	2	96%	?
9	50006 (1995-10-15) - 50226 (1996-05-22)	221	11	152	2	84%	?
10	50391 (1996-11-03) - 50595 (1997-05-26)	205	12	148	1	65%	-
11	50736 (1997-10-14) - 50955 (1998-05-21)	220	13	134	1	59%	+
12	51103 (1998-10-16) - 51325 (1999-05-26)	223	8	188	2	85%	?, /
13	51474 (1999-10-22) - 51687 (2000-05-22)	214	10	126	3	95%	+
14	51861 (2000-11-12) - 52052 (2001-05-22)	192	11	73	1	92%	?, /
15	52214 (2001-10-31) - 52421 (2002-05-26)	208	19	81	2	93%	?, /
16	52582 (2002-11-03) - 52785 (2003-05-25)	204	12	100	3	97%	-/
17	52977 (2003-12-03) - 53149 (2004-05-23)	173	9	85	2	94%	-
18	53299 (2004-10-20) - 53506 (2005-05-15)	208	21	92	2	94%	-
19	53660 (2005-10-16) - 53876 (2006-05-20)	217	10	107	2	97%	-
20	54044 (2006-11-04) - 54238 (2007-05-17)	195	8	101	2	99%	-
21	54400 (2007-10-26) - 54599 (2008-05-12)	200	13	124	3	98%	-
22	54761 (2008-10-21) - 54966 (2009-05-14)	206	25	70	2	96%	?, /
23	55121 (2009-10-16) - 55312 (2010-04-25)	192	15	97	2	95%	-
24	55499 (2010-10-29) - 55690 (2011-05-08)	191	6	127	2	90%	+
25	55875 (2011-11-09) - 56054 (2012-05-06)	179	12	116	3	99%	-
26	56226 (2012-10-25) - 56426 (2013-05-13)	200	95	44	1	77%	?
27	56589 (2013-10-23) - 56783 (2014-05-05)	194	60	70	2	94%	?

**Table 2.** Summary of the local CF analysis results. Columns from left to right: segment number, start and end time epochs for the segment in HJD - 2400000 and corresponding dates, length of the segment in days  $\Delta T_{seg}$ , length of the longest gap  $\Delta T_{gap}$  in days, number of observations  $N$ , number of modulators  $L$ , goodness of fit  $R^2$  and the type of the event that could be detected in the segment (if any). NA stands for the segment having not enough data points for meaningful CF analysis, '-' for smooth phase behavior, '+' for disrupted phase behavior of flip-flop type, '?' for disrupted phase behavior that can not be associated with a flip-flop type event, '/' phase drifts.

and smaller blue dots represent the locations of primary and secondary minima respectively. As noted above, 1000 bootstrap samples were calculated for the global CF to obtain error estimates for the minima. However, for a clearer visualization these are omitted from the figure, but are included in the online material, where the global CF solution is given.

In Cole et al. (2014a) the DI technique was applied to spectrometry of 7 observing seasons. The resulting surface temperature maps were used to determine the epochs of the temperature minima, interpreted as starspots, for every season. Especially high activity level, i.e. a large amount of cool spots, was observed to occur during October 1999 to November 2000. In Fig. 10 we have plotted the retrieved spot epochs with orange circles, where the size of the circle reflects the temperature of the given spot (a larger circle corresponds to a lower temperature). On the same plot we have also included the minima obtained from the CPS method published in Lehtinen et al. (2012). Red pluses and blue crosses respectively represent the primary and secondary minima.

As expected the minima obtained from the global fit serve as the averaged values for the minima obtained from the CPS. Agreement with the results from DI is also quite satisfactory. There is a quite good match between DI and other models for some of the minima found in seasons 3 to 7. Even though neither active longitudes nor flip-flop type events were seen in DI, both global and local CF analysis

reveal a possible flip-flop. However, it is not reasonable to search for the full agreement between photometry and DI. For instance the photometry is affected by the limb darkening and surface area projection effects of the active regions, so that one to one correspondence between the strongest minima in photometry and the lowest temperature regions in DI cannot be expected. We also note that the observing seasons for spectrometry and photometry mostly do not overlap. In addition a low S/N ratio as well as less than ideal phase coverage for several observing seasons was reported, which increases the uncertainties even further (Cole et al. 2014a).

## 6. Discussion

If we make an assumption that the scatter around the mean period is the result of differential rotation we can use the half-width of the minimum as an approximation for the standard deviation. Based on this we can estimate the differential rotation coefficient using the formula by Jetsu (1993):

$$k = \frac{6\Delta P_0^{D2}}{P_0^{D2}}, \quad (12)$$

where in our case  $\Delta P_0^{D2} \approx 0.0084$  is taken as the  $\sigma$  of the closest gaussian curve to dispersion statistic with correlation length of 100 days. Substituting the value into the equation leads to  $k \approx 0.032$  which is in

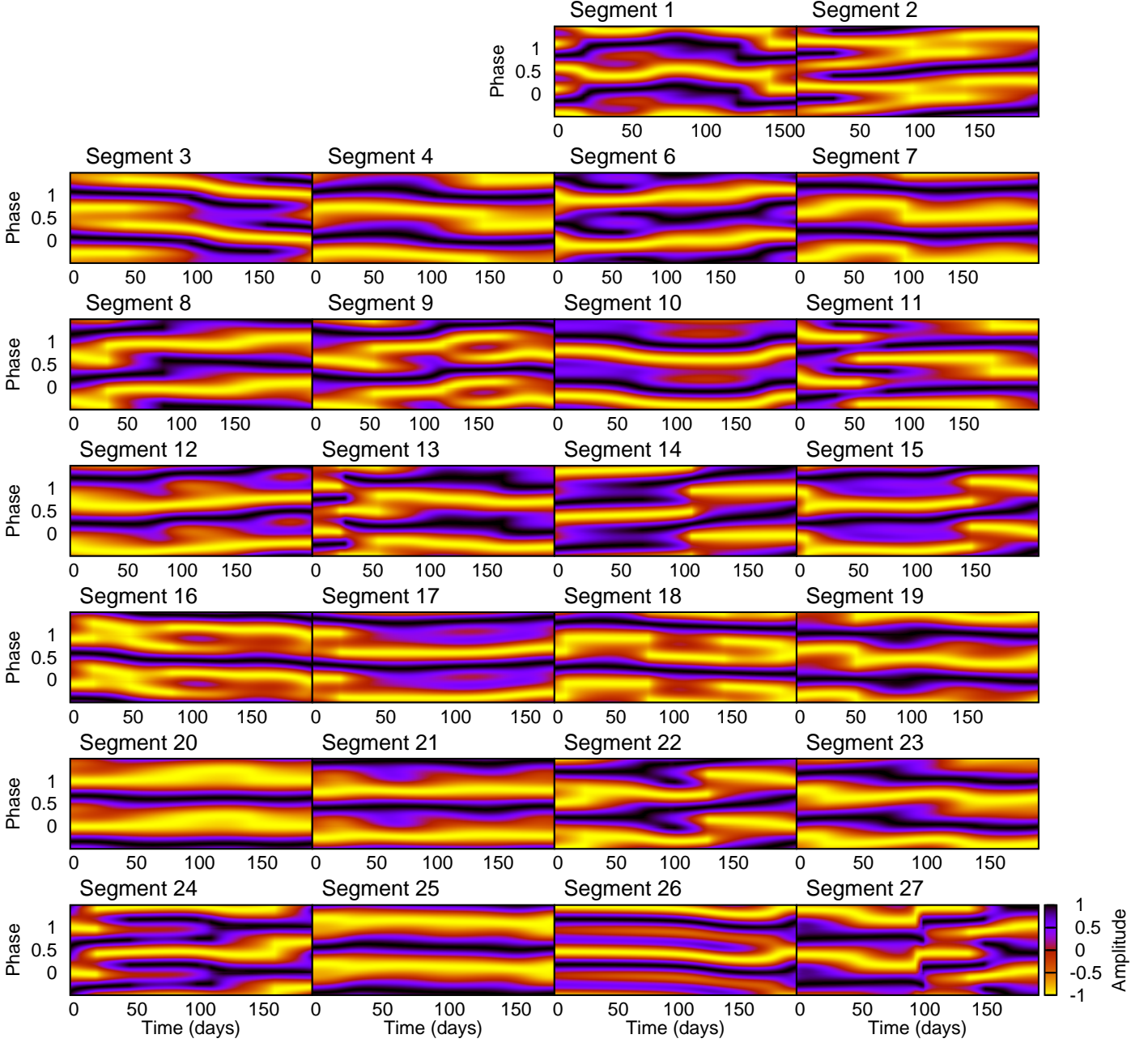


**Fig. 9.** Phase diagrams of local fits with refined carrier period  $P_0^{D2} = 1^d60514$

rough agreement with previous estimates from photometry (e.g. Lehtinen et al. 2012; You 2007; Jetsu 1993),  $k=0.015\dots0.025$ , but significantly larger than the values obtained from DI (Kovári et al. 2004; Donati et al. 2003b, e.g.),  $k=0.002\dots0.006$ .

The Coriolis number is an estimate of the strength of the rotational influence over turbulent convection, and can be written as (Saar & Brandenburg 1999)

$$\text{Co} = 4\pi\tau_c/P_{\text{rot}}, \quad (13)$$

where  $P_{\text{rot}}$  is the rotation period of the star and  $\tau_c$  is the convective turnover time. Ossendrijver (1997) pre-

sented an extrapolation method to the theoretical calculations of Kim & Demarque (1996), to estimate the convective turnover time from the B-V index. Lehtinen et al. (2012) applied this technique and arrived at an estimate of  $\tau_c \approx 33.5$  days for LQ Hya. On the other hand, they used their CPS method to compute the time scale of change, denoted with  $T_c$ , for each individual data set investigated, and as an average of all the analyzed segments, found a value of 50.5 days. As this quantity describes the typical time in which changes in spot configuration occur, it can be postulated to have some relation to the convective turnover time.

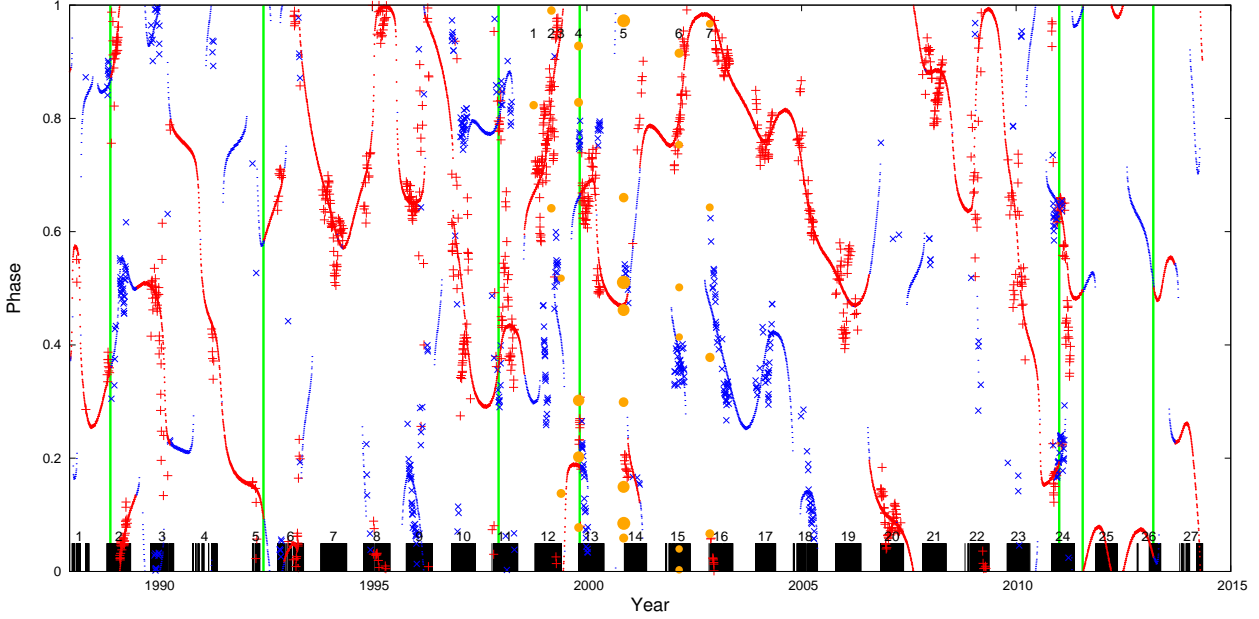


**Fig. 10.** Phases of the minima for period  $P_0^{D2}=1^d60514$ . Red dots: primary minima from CF, red pluses: primary minima from CPS, blue points: secondary minima from CF, blue crosses: secondary minima from CPS, orange circles: minima from DI, bold green vertical lines denote the epochs of possible flip-flop events. The black bars with the numbers correspond to the photometric observing seasons, the numbers on top of the figure mark the observing seasons of DI.

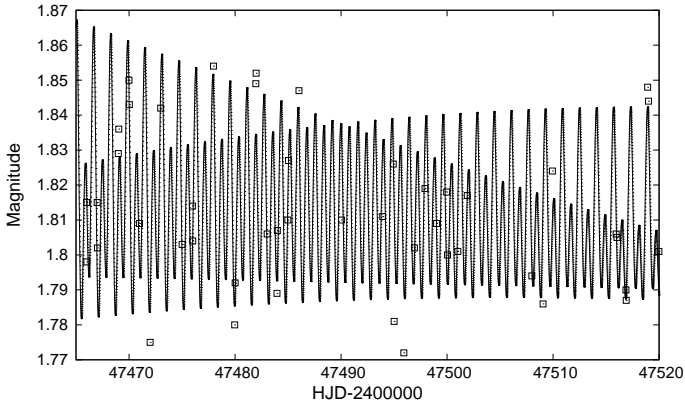


**Fig. 11.** Zoom-in to the global CF near the flip-flop event detected in the segment 2. The data points are drawn as small rectangles.

The Coriolis number of LQ Hya, based on the above stated values of the turnover time, lies within the range 260-400, these numbers being huge in comparison to the Sun with  $Co$  of roughly 6 with the definition Eq. (13). In the study of Saar & Brandenburg (1999) stars were observed to cluster on certain activity branches, when their Coriolis number and rotational vs. magnetic cycle periods,  $P_{rot}/P_{cyc}$ , were plotted. LQ Hya was termed as an anomalous object, falling in the transition region between the active (A) and superactive (S) branches, based on the values  $\tau_c \approx 20.9$  days by Gunn et al. (1998) and  $P_{cyc} \approx 7$  years by Strassmeier et al. (1997) used back then. The majority of magnetic cycle determinations still falling into the

range of 6-7 years, together with the usage of the alternative methods to determine the convective turnover time to compute the Coriolis number, would place the object to an even more anomalous place in the diagnostic diagram, clearly further away from the other stars (although only a few of them identified) in the transition region. This makes LQ Hya a very fascinating object to follow up and study further. These considerations, on the other hand, might also indicate that the division into active and superactive branches in the diagnostic diagram is not as meaningful as the separation into the inactive and active ones (the so-called Vaughan-Preston gap).

The difference between the retrieved mean rotation period of the star and the most pronounced coherent phase structure during 2005 and 2008 ( $P_{coh} = 1^d6037$ ) is roughly 0.00171 days. During the aforementioned years, the trend in the phase-time diagram is nearly linear, the spot structure going faster (nearly linear downward trend) with respect to the mean rotation of spots. Previously, such behavior has been seen on more evolved rapid rotators (Lindborg et al. 2011; Hackman et al. 2013), and has been interpreted as being due to either latitudinal differential rotation or an azimuthal dynamo wave. The effect is definitely the clearest in the primary component of the binary system II Peg, where a clear linear trend is visible for over ten years (see e.g. Lindborg et al. 2013), whereas only disrupted up- and downward trends were seen in the single giant FK Com (Hackman et al. 2013). The complexity level and the type of phase behavior seen in FK Com are similar to the ones reported for LQ Hya in the present paper; this could be an indication of the binarity of II Peg having an influence on stabilizing the active longitudes in comparison to single stars, LQ Hya and FK Com representing this class.

In the case of II Peg and FK Com, however, it was difficult to definitely rule out the differential rotation scenario, as for instance in the case of II Peg, similar magnitude of drift could have been caused by an anti-solar differential rotation profile with  $k$  comparable to the values deduced from observations. Also, in the case of LQ Hya, the situation is somewhat similar: the deduced values of the differential rotation parameter  $k$  range between 0.002 ... 0.032, the smallest ones being obtained from Doppler imaging, the largest ones from photometry. DI and ZDI studies (e.g. Strassmeier et al. 1993; Rice & Strassmeier 1998; Donati 1999; Donati et al. 2003b; Kovári et al. 2004; Cole et al. 2014a) indicate that the majority of the spot activity of LQ Hya occurs at two different latitudinal regions, namely at high- and nearly equatorial regions. It cannot be ruled out that in such a system, spots could be drifting from the high-latitude location to the lower-latitude one, in which case they would gradually attain faster rotation rate due to the most likely solar-like rotation law of the object. The maximal latitude range of the drifting structure versus the mean spot latitude would be of the order of  $\pi/4$ , and therefore the implied  $k$  for the spot structures roughly half of the differential rotation parameter, i.e.  $k_{\text{dr}}^{\text{exp}} = 0.001 \dots 0.016$ . The value that can be directly computed from the period difference of the coherent structure and the mean movement of the spots reads

$$k_{\text{dr}}^{\text{drift}} = \frac{P_0^{\text{D}2} - P_{\text{coh}}}{P_0^{\text{D}2}} \approx 1.1 \times 10^{-3}, \quad (14)$$

which is close to the lower limit of the values derived from Doppler imaging. Therefore, again, there is certainly enough differential rotation on the object to be the cause of the observed phase-time drift. One must note that such a drift would not cause strictly linear (but curved) trends in the phase-time plots (see Pelt et al. 2011, for a simulated example). One should also expect drifts from the lower latitude spot band to the higher one, with opposite direction of the trend in the phase-time plots. These are indeed seen, but with less pronounced phase coherence.

In Alekseev (2005) it was also proposed, based on photometric spot modeling, that a latitudinal dynamo wave, the spot activity migrating from the equator poleward (the solar butterfly reversed), is present on the object. The analysis of Lehtinen et al. (2012) did not reveal such trends, nor does the CF analysis picture of linear down- or upward trends support this picture.

The phase behavior, if not due to differential rotation nor latitudinal dynamo waves, could also be a manifestation of an azimuthal dynamo wave, predicted to be excited in rapid rotators (e.g. Krause & Raedler 1980), verified from mean-field dynamo models (e.g. Moss et al. 1995; Küker & Rüdiger 1999; Mantere et al. 2013), and now also found from direct numerical simulations (Cole et al. 2014b). Such dynamo waves most often behave as if detached from the overall rotation of the object, moving with a different speed than the stellar surface. Their rotation is rigid even in a differentially rotating object. Therefore, a systematic linear phase drift could most directly be linked to the presence of azimuthal dynamo waves. Dynamo theory, on the other hand, serves no direct explanation as to why the linear trends are broken and reversed, which is clearly the case for LQ Hya.

## 7. Conclusions

In this work we have presented analysis of LQ Hya photometry for 1982-2014. Several different statistical methods were first used to nail down a suitable carrier frequency for our main analysis tool, the CF method. From this preliminary analysis we learned several interesting aspects:

Firstly, there is a certain cut-off in the spectrum at the high frequency end. This can be interpreted as a limiting value for the spot cycle length at the low latitudes or near the equator of the star. Second interesting feature appearing as the result of the same analysis is the bimodal shape of the spectrum. The explanation for this can be searched from different causes e.g. latitudinal distribution of the spots. From DI maps for LQ Hya it has become evident that spot regions tend to lie either on high or low latitudes while there seems to be spotless area on mid-latitude range (Cole et al. 2014a; Donati et al. 2003b). Other possible explanations might be either radial differential rotation manifesting itself through different anchoring depths for spots or hemispherical asymmetry.

In previous studies the focus has been on searching for active longitudes on the star (Jetsu 1993; Berdyugina et al. 2002; Kovári et al. 2004; Lehtinen et al. 2012). Here we took a different approach by estimating the mean rotation period of the spot structures on the star using the phase dispersion statistic  $D^2(P)$ . This period is a close analogue to the Carrington rotation period of the Sun. In subsequent CF analysis we used the obtained value as a carrier period and produced the corresponding phase plots. We noticed shorter and longer, nearly linear, trends with different slopes reflecting the "duty times" of certain periods during these time frames. Especially pronounced are two epochs (1991–1993; 2005–2008) with a downward trend. The overall picture is inconsistent with the antisolar butterfly diagram postulated by Alekseev (2005). The possible sources of these trends include disrupted azimuthal dynamo waves and solar-like latitudinal differential rotation.

We also tried a multiperiodic model to describe the photometry of LQ Hya. This however led to low  $R^2$  values and the regular structure of the simple model was lost in the phase diagram of the CF. Therefore we concluded this model to be barely suitable. Interestingly enough, this analysis gave a phase modulation period of roughly 6.94 years, a value also derived from the mean brightness variation of the star.

From the global CF we calculated the phases of the minima and compared them with the results obtained by Lehtinen et al. (2012) using the CPS method. These two models appeared to be in good agreement. Comparison with the results by Cole et al. (2014a) using DI technique was challenging due to the non-overlapping of the corresponding observing seasons. However, around late 1999 and late 2000 rough agreement between the epochs of the photometric minima and the DI spots can be seen.

Qualitative analysis of the local CF was done for 27 observing seasons. We detected 4 flip-flop type events from the phase plots, 3 of these matching with the epochs of flip-flops obtained from the global CF. The timing of the events appears to be random which excludes the possibility of the 5.2 year cycle reported by Berdyugina et al. (2002). Comparison of the phase plots with the ones reported by Lehtinen et al. (2012) showed a good agreement – majority of features can be detected from both analysis.



*Acknowledgements.* This work has been supported by the Academy of Finland Centre of Excellence ReSoLVE (NO, MM, JP). The work of TH was financed through the project Active Suns by the University of Helsinki. G.W.H. acknowledges long-term support from Tennessee State University and the State of Tennessee through its Centers of Excellence program.

## References

- Alekseev, I. Y. 2005, *Astrophysics*, 48, 20
- Barnes, J. R., Collier Cameron, A., Donati, J.-F., et al. 2005, *MNRAS*, 357, L1
- Barning, F. J. M. 1963, *Bull. Astron. Inst. Netherlands*, 17, 22
- Berdyugina, S. V., Pelt, J., & Tuominen, I. 2002, *A&A*, 394, 505
- Cole, E., Hackman, T., Käpylä, M. J., et al. 2014a, *A&A*, submitted
- Cole, E., Käpylä, P. J., Mantere, M. J., & Brandenburg, A. 2014b, *ApJ*, 780, L22
- Covino, S., Panzera, M. R., Tagliaferri, G., & Pallavicini, R. 2001, *A&A*, 371, 973
- Cutispoto, G. 1991, *A&AS*, 89, 435
- Cutispoto, G. 1998, *A&AS*, 131, 321
- Donati, J.-F. 1999, *MNRAS*, 302, 457
- Donati, J.-F., Collier Cameron, A., & Petit, P. 2003a, *MNRAS*, 345, 1187
- Donati, J.-F., Collier Cameron, A., Semel, M., et al. 2003b, *MNRAS*, 345, 1145
- Eggen, O. J. 1984, *AJ*, 89, 1358
- Fekel, F. C., Bopp, B. W., Africano, J. L., et al. 1986, *AJ*, 92, 1150
- Gunn, A. G., Mitrou, C. K., & Doyle, J. G. 1998, *MNRAS*, 296, 150
- Hackman, T., Pelt, J., Mantere, M. J., et al. 2013, *A&A*, 553, A40
- Jetsu, L. 1993, *A&A*, 276, 345
- Kim, Y.-C. & Demarque, P. 1996, *ApJ*, 457, 340
- Kitchatinov, L. L. & Olemskoy, S. V. 2011, *MNRAS*, 411, 1059
- Kovári, Z., Strassmeier, K. G., Granzer, T., et al. 2004, *A&A*, 417, 1047
- Krause, F. & Raedler, K. H. 1980, *Mean-field magnetohydrodynamics and dynamo theory*
- Küker, M. & Rüdiger, G. 1999, *A&A*, 346, 922
- Lehtinen, J., Jetsu, L., Hackman, T., Kajatkari, P., & Henry, G. W. 2011, *A&A*, 527, A136
- Lehtinen, J., Jetsu, L., Hackman, T., Kajatkari, P., & Henry, G. W. 2012, *A&A*, 542, A38
- Lindborg, M., Korpi, M. J., Hackman, T., et al. 2011, *A&A*, 526, A44
- Lindborg, M., Mantere, M. J., Olsper, N., et al. 2013, *A&A*, 559, A97
- Lomb, N. R. 1976, *Ap&SS*, 39, 447
- Mantere, M. J., Käpylä, P. J., & Pelt, J. 2013, in *IAU Symposium*, Vol. 294, *IAU Symposium*, ed. A. G. Kosovichev, E. de Gouveia Dal Pino, & Y. Yan, 175–186
- McIvor, T., Jardine, M., Collier Cameron, A., Wood, K., & Donati, J.-F. 2004, *MNRAS*, 355, 1066
- Messina, S. & Guinan, E. F. 2003, *A&A*, 409, 1017
- Moss, D., Barker, D. M., Brandenburg, A., & Tuominen, I. 1995, *A&A*, 294, 155
- Oláh, K., Kolláth, Z., Granzer, T., et al. 2009, *A&A*, 501, 703
- Oláh, K., Kolláth, Z., & Strassmeier, K. G. 2000, *A&A*, 356, 643
- Ossendrijver, A. J. H. 1997, *A&A*, 323, 151
- Pelt, J. 1983, in *ESA Special Publication*, Vol. 201, *Statistical Methods in Astronomy*, ed. E. J. Rolfe, 37–42
- Pelt, J., Olsper, N., Mantere, M. J., & Tuominen, I. 2011, *A&A*, 535, A23
- Reinhold, T. & Reiners, A. 2013, *A&A*, 557, A11
- Rice, J. B. & Strassmeier, K. G. 1998, *A&A*, 336, 972
- Saar, S. H. & Brandenburg, A. 1999, *ApJ*, 524, 295
- Saar, S. H., Piskunov, N. E., & Tuominen, I. 1994, in *Astronomical Society of the Pacific Conference Series*, Vol. 64, *Cool Stars, Stellar Systems, and the Sun*, ed. J.-P. Caillault, 661–663
- Scargle, J. D. 1982, *ApJ*, 263, 835
- Stellingwerf, R. F. 1978, *ApJ*, 224, 953
- Strassmeier, K. G., Bartus, J., Cutispoto, G., & Rodono, M. 1997, *A&AS*, 125, 11
- Strassmeier, K. G., Rice, J. B., Wehlau, W. H., Hill, G. M., & Matthews, J. M. 1993, *A&A*, 268, 671
- Tetzlaff, N., Neuhäuser, R., & Hohle, M. M. 2011, *MNRAS*, 410, 190
- White, R. J., Gabor, J. M., & Hillenbrand, L. A. 2007, *AJ*, 133, 2524
- You, J. 2007, *A&A*, 475, 309